Modeling variations of summer upper tropospheric temperature and associated climate over the Asian Pacific region during the mid-Holocene

Botao Zhou[1,2] and Ping Zhao[3]

[1]   The summer upper tropospheric temperature change and its association with atmospheric circulations and precipitation over the Asian Pacific region during the mid-Holocene have been addressed by using outputs from a coupled ocean atmosphere general circulation model performed as part of the second phase of the Paleoclimate Modeling Intercomparison Project. The simulated result shows the summer oscillation pattern similar to the present Asian Pacific oscillation (APO) existed in the mid-Holocene. When there was a warming (cooling) upper troposphere over East Asia, a cooling (warming) upper troposphere occurred over the midlatitudes of the North Pacific. Compared to the modern climate, however, the simulated mid-Holocene temperature in the upper troposphere was higher over East Asia and lower over the midlatitudes of the North Pacific, indicating a stronger summer APO in the mid-Holocene. Corresponding to such a condition, the North Pacific was modeled to be dominated by a high-level cyclonic circulation difference and a low-level anticyclonic circulation difference in the mid-Holocene relative to the present, which favored the subsidence of airflows and thus resulted in less precipitation in this region. Meanwhile, East Asia was simulated to be occupied by an anticyclonic circulation difference in the upper troposphere and a cyclonic circulation difference in the lower troposphere. Accordingly, the ascending motion and the low-level southerly wind strengthened in East Asia, leading to an increase of local precipitation in the mid-Holocene. Therefore, the modeled mid-Holocene climate suggests that the summer rainfall change over the Asian Pacific region may be a result of the strengthened APO in the upper troposphere.

1.   Introduction

[2] The climate during the mid-Holocene (6000 years before present), which is one of the focuses of the Paleoclimate Modeling Intercomparison Project (PMIP), was largely different from the present. This difference, to a large extent, is attributed to variations of the solar insolation because of changes in Earth's orbital parameters. The Northern Hemispheric insolation in the mid-Holocene increased by about 5% in summer and decreased by a similar amount in winter [*Berger*, 1978]. Consequently, the Northern Hemisphere summers during the mid-Holocene were warmer than today.

[3]   Climate models were extensively applied to reproduce the mid-Holocene climate and to understand the reasons of the mid-Holocene climate change. In the first phase of PMIP (PMIP1), numerous mid-Holocene climate simulations were performed by use of atmospheric general circulation models [e.g., *Kutzbach and Guetter*, 1986; *de Noblet et al.*, 1996; *Kutzbach et al.*, 1996; *Claussen and Gayler*, 1997; *Hall and Valdes*, 1997; *Joussaume et al.*, 1999; *Wang*, 1999, 2000, 2002]. These studies generally revealed that the change in solar insolation primarily drove the expansion of the Asian and African summer monsoons. However, these simulations cannot fully explain observed vegetation and hydrological changes in the Afro-Asian monsoon regions [*Yu and Harrison*, 1996; *Harrison et al.*, 1998; *Coe and Harrison*, 2002; *Bonfils et al.*, 2004]. So fully coupled ocean atmosphere general circulation models (OAGCMs) have been exploited to address the mid-Holocene climate and ocean feedback in recent years, particularly under the second phase of PMIP (PMIP2) framework [e.g., *Liu et al.*, 2003a, 2003b, 2004; *Levis et al.*, 2004; *Wohlfahrt et al.*, 2004, 2008; *Renssen et al.*, 2005; *Otto-Bliesner et al.*, 2006; *Ohgaito and Abe-Ouchi*, 2007; *Wang et al.*, 2008; *Marzin and Braconnot*, 2009a, 2009b; *Dallmeyer et al.*, 2010]. An overview of the PMIP2 OAGCM simulations was given by

[1]Nansen-Zhu International Research Center, Institute of Atmospheric Physics, Chinese Academy of Sciences, Beijing, China.
[2]National Climate Center, China Meteorological Administration, Beijing, China.
[3]National Meteorological Information Center, China Meteorological Administration, Beijing, China.

Braconnot et al. [2007a, 2007b], who showed that the PMIP2 simulations were, in general, in better agreement with proxy data than the PMIP1 simulations. Ocean-atmosphere interaction could amplify the orbitally forced signal and further enhance the North African monsoon [*Kutzbach and Liu*, 1997; *Hewitt and Mitchell*, 1998; *Braconnot et al.*, 2000; *Liu et al.*, 2004; *Zhao et al.*, 2005; *Braconnot et al.*, 2007a; *Marzin and Braconnot*, 2009a]. Besides, several studies highlighted a dampening of the Asian monsoon due to ocean feedback [*Voss and Mikolajewicz*, 2001; *Liu et al.*, 2004; *Ohgaito and Abe-Ouchi*, 2007; *Marzin and Braconnot*, 2009b; *Dallmeyer et al.*, 2010].

[4] The East Asian summer monsoon is an important and complex phenomenon in eastern China and the western Pacific, generally characterized by the low-level southwesterly wind or southeasterly wind over these regions and driven by zonal and meridional thermal contrasts between the East Asian land and the adjacent oceans [*Chen et al.*, 1991; *He et al.*, 2007; *Zhao et al.*, 2010]. When the summer thermal contrasts strengthen, the southerly wind moves more northward, indicating a strong East Asian summer monsoon circulation. Accordingly, the monsoonal rain belt in front of the maximum southerly wind shifts northward, accompanying more rainfall over northern China and less rainfall over southern China.

[5] Studies on the modern climate indicated that there is an opposite variation in the tropospheric temperature between East Asia and the North Pacific. When the troposphere is warming (cooling) over the Asian continent, the troposphere is cooling (warming) over the North Pacific. This out-of-phase relationship is called the Asian Pacific oscillation (APO) [*Zhao et al.*, 2007]. Such a zonal seesaw pattern may indicate variability of thermal contrasts between Asia and the North Pacific as well as East Asian monsoon circulation and monsoonal precipitation. For example, during the past 40 years, the tropospheric temperature exhibited a cooling trend over East Asia and a warming trend over the North Pacific in summer, weakening the thermal contrast in the extratropics and thus resulting in the weakened East Asian summer monsoon and producing the southern floods/northern droughts over eastern China [*Zhao et al.*, 2010].

[6] The formation of APO is associated with the zonal vertical circulation that is possibly caused by the difference of the solar radiative heating between the Asian continent and the North Pacific Ocean [*Zhao et al.*, 2008]. Because the solar forcing in the mid-Holocene differed from the present, we wonder whether APO occurred in the mid-Holocene and how the mid-Holocene APO was associated with the atmospheric circulation and climate. With these questions in mind, we examine APO and associated atmospheric circulation and precipitation based on a coupled climate model (CCSM3), and we compare them with the present climate. The CCSM3 model can simulate a stronger summer monsoonal precipitation in North Africa and a warmer summer surface temperature over North America, Eurasia, and northern Africa in the mid-Holocene relative to today [*Otto-Bliesner et al.*, 2006], consistent with the proxy data [*Jolly et al.*, 1998; *Prentice et al.*, 2000]. Over East Asia, CCSM3 simulated a stronger East Asian summer monsoon, a higher summer surface temperature, and a northwestward monsoonal rain belt in China during the mid-Holocene as compared to the present [*Zhou and Zhao*, 2009]. A more detailed comparison between the mid-Holocene simulations and the reconstructed data in China was given by *Wang et al.* [2010], which revealed a good agreement between the simulations and the reconstructed data in summer surface temperature over East China and summer precipitation in most part of China during the mid-Holocene. These results suggest that CCSM3 model can generally capture the pronounced features of the mid-Holocene climate and may be used to simulate the Asian Pacific climate in the mid-Holocene.

[7] The rest of the paper is organized as follows. Section 2 describes the model and experiment design. In section 3, we investigate the tropospheric temperature teleconnection over the Asian Pacific region from the observed and modeled results. We also examined the changes of atmospheric circulation and precipitation in association with this teleconnection. Finally, a summary and discussion are provided in section 4.

2. Model and Experiments

[8] The CCSM3 model is a global coupled ocean-atmosphere climate model [*Collins et al.*, 2006a]. It includes National Center for Atmospheric Research Community Atmospheric Model version 3 (NCAR CAM3) with the approximately horizontal resolution of 2.8° latitude by 2.8° longitude and 26 hybrid coordinate levels in the vertical [*Collins et al.*, 2006b] as the atmospheric component and the NCAR Parallel Ocean Program (POP) model with a nominal grid spacing of approximately 1° in latitude and longitude [*Gent et al.*, 2006] as the oceanic component.

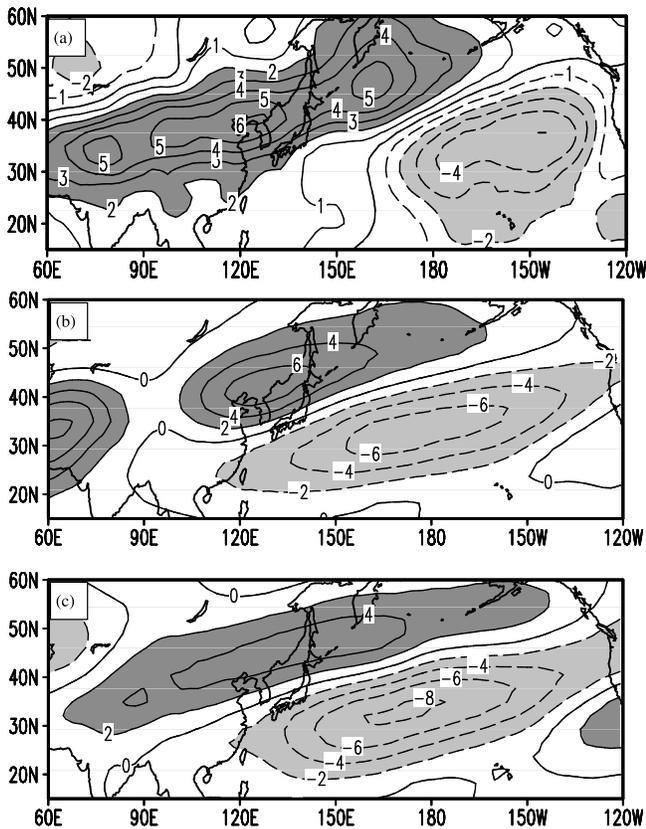[9] Following the PMIP2 protocol (see http://pmip2.lsce.ipsl.fr/), the mid-Holocene simulation (6ka) is performed with the mid-Holocene orbital parameters derived from *Berger* [1978] and an atmospheric CH_4 concentration of 650 ppb. The present-day simulation (0ka) is done with the present orbital parameters and an atmospheric CH_4 concentration of 760 ppb. For both periods, the CO_2 and N_2O concentrations are, respectively, set to 280 and 270 ppb, and other boundary conditions are the same. The output over the last 100 years, archived in the PMIP2 database (http://pmip2.lsce.ipsl.fr/), is used in this study.

[10] Since the tropospheric temperature mainly exhibits a meridional difference and generally decreases from the equator to the pole, we use a 500–300 hPa mean eddy air temperature (T') to represent upper tropospheric eddy temperature in which $T' = T - [T]$, T is the air temperature, and $[T]$ is the zonal mean of T. The summer refers to June–July–August. The statistic significance of the difference between 6ka and 0ka simulations is assessed by the Student's t test.

3. Results

3.1. Upper Tropospheric Temperature Variations

[11] We first examine the spatial distribution of upper tropospheric (500–300 hPa) T' using an empirical orthogonal function (EOF) analysis over the Asian Pacific region from the reanalysis data [*Uppala et al.*, 2005] for the period 1961–2000. The first EOF mode (hereafter EOF1) accounts for 21% of the total variance, and the second EOF mode (hereafter EOF2) accounts for 12%. The observed EOF1 pattern (Figure 1a) exhibits positive values over the mid-

Figure 1. The first empirical orthogonal function mode (in 10^{-2} °C) of the summer upper tropospheric (500–300 hPa) T' for (a) the European Centre for Medium-Range Weather Forecasts reanalysis data during 1961–2000, (b) the 0ka simulation, and (c) the 6ka simulation. Heavy (light) shading denotes T' values higher (lower) than 0.02°C (−0.02°C).

latitudes of Asia and negative values over the extratropical North Pacific. Correlation analysis further shows that the East Asian positive center (80–140°E, 35–55°N) has a correlation of −0.54 with the North Pacific negative center (160°E–130°W, 20–40°N). Thus, both the EOF and correlation analyses indicate that high (low) upper tropospheric T' over East Asia accompanies low (high) upper tropospheric T' over the midlatitudes of the North Pacific. This teleconnection is the so-called APO phenomenon [*Zhao et al.*, 2007].
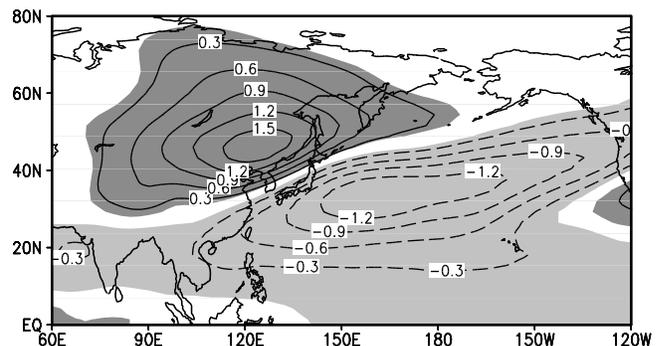
[12] Similarly, we perform an EOF analysis of the summer T' from the CCSM3 simulations. In the 0ka simulation, the EOF1 and EOF2, respectively, explain 23 and 14% of the total variance. The EOF1 mode in the 0ka simulation (Figure 1b) indicates an opposite variation of T' between Asia and the North Pacific, with the positive center over East Asia and the negative center over the midlatitudes of the North Pacific, consistent with the observation (Figure 1a), although the simulated negative center moves slightly westward. Thus, the feature of the observed upper tropospheric atmospheric oscillation over the Asian Pacific region can be generally captured by CCSM3. In the 6ka simulation, the variance of EOF1 and EOF2 are 21 and 11%, respectively. The EOF1 pattern in the 6ka simulation (Figure 1c) is

similar to that in the 0ka simulation (Figure 1b), hinting that the opposite variation in tropospheric temperature over the Asian Pacific region also occurred in the mid-Holocene. For convenience, this simulated relationship is still called the APO.
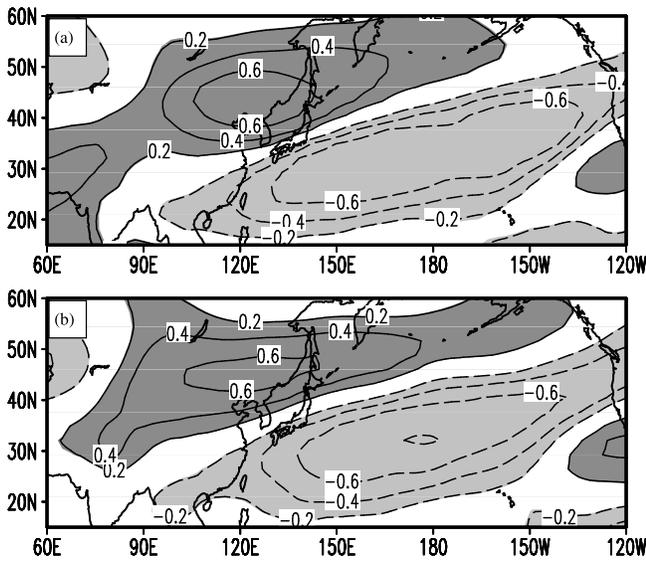
[13] However, there are some significant differences in the APO between 6ka and 0ka simulations. Figure 2 shows the composite difference of the summer upper tropospheric T' between 6ka and 0ka simulations. It appears that the difference pattern resembles the EOF1 modes shown in Figure 1, with the positives mainly over East Asia and the negatives mainly over the midlatitudes of the North Pacific. This modeling result implies a warmer (colder) upper tropospheric T' over East Asia (the North Pacific) and a stronger thermal contrast in the troposphere between East Asia and the North Pacific during the mid-Holocene with respect to the present.

[14] Referring to the positions of the positive and negative centers in two simulations, we define the East Asian T' index (EAI) and the North Pacific T' index (NPI) as the upper tropospheric T' averaged over the regions (80–140°E, 35–55°N) and (150°E–150°W, 20–40°N), respectively, to measure variations of the simulated T' intensity over East Asia and the North Pacific. A correlation analysis shows that the EAI is significantly correlated to the NPI, with the correlation coefficient of −0.43 (−0.44) in the 0ka (6ka) simulation for 100 years, further supporting the observed result and demonstrating that the upper tropospheric T' over East Asia does covary with that over the midlatitudes of the North Pacific in both the present and the mid-Holocene. Thus, we define an index of APO (hereafter APOI) as an arithmetic difference between the East Asian and North Pacific T' indices; that is, $APOI = T'_{80-140°E,\ 35-55°N} - T'_{150°E-150°W,\ 20-40°N}$. The APOI has a significant positive correlation of 0.85 (0.84) with the EAI and a significant negative correlation of −0.84 (−0.85) with the NPI for 0ka (6ka), and can well represent the variations of the East Asian and North Pacific T' indices and the difference between them.

[15] Figure 3 depicts the correlations between the APOI and the 500–300 hPa mean T' field. In Figure 3, significant positive correlations over East Asia and significant negative correlations over the midlatitudes of the North Pacific are evident at both 0ka and 6ka. Such a correlation pattern is also consistent with the EOF1 pattern shown in Figure 1. Meanwhile, the APOI is highly correlated to the time series

Figure 2. Composite difference of the summer upper tropospheric T' (in °C) between 6ka and 0ka. Areas above 95% significance level are shaded.

Figure 3. Correlations between the Asian Pacific oscillation index and the upper tropospheric T' field in summer at (a) 0ka and (b) 6ka. Areas above 95% significance level are shaded.
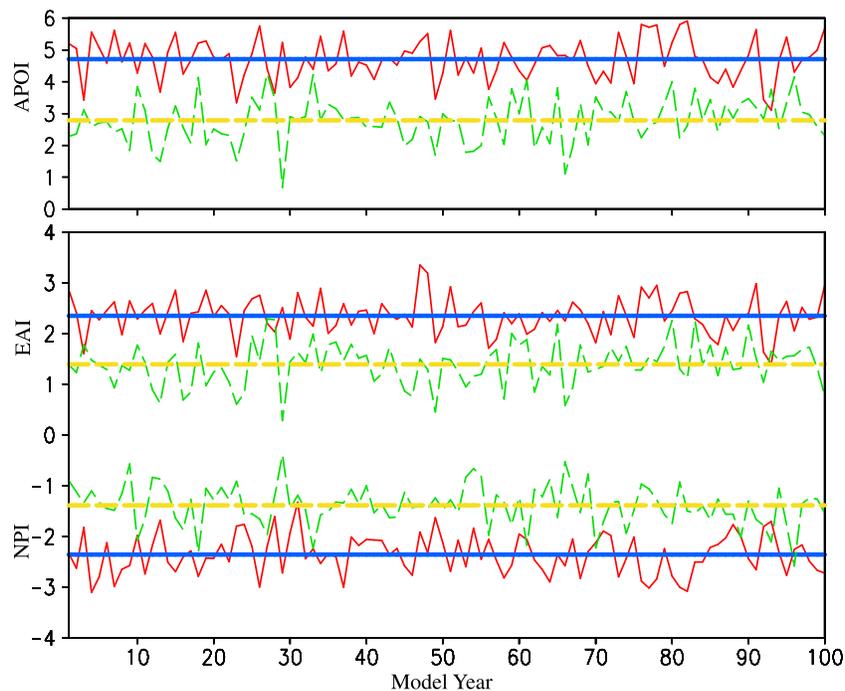
of the EOF1 mode, with the correlation coefficient of 0.87 (0.92) at 0ka (6ka), implying the robustness of using APOI as a proxy for the time series of the EOF1 mode at the present and in the mid-Holocene. Figure 4 delineates temporal variations of the EAI, NPI, and APOI in the 0ka and 6ka simulations. The mean values of the EAI, NPI, and APOI are 2.35°C, −2.36°C, and 4.71°C at 6ka, while they are 1.39°C,

−1.39°C, and 2.78°C at 0ka in turn. All these indices were bigger in the mid-Holocene than today, in agreement with the result from Figure 2.
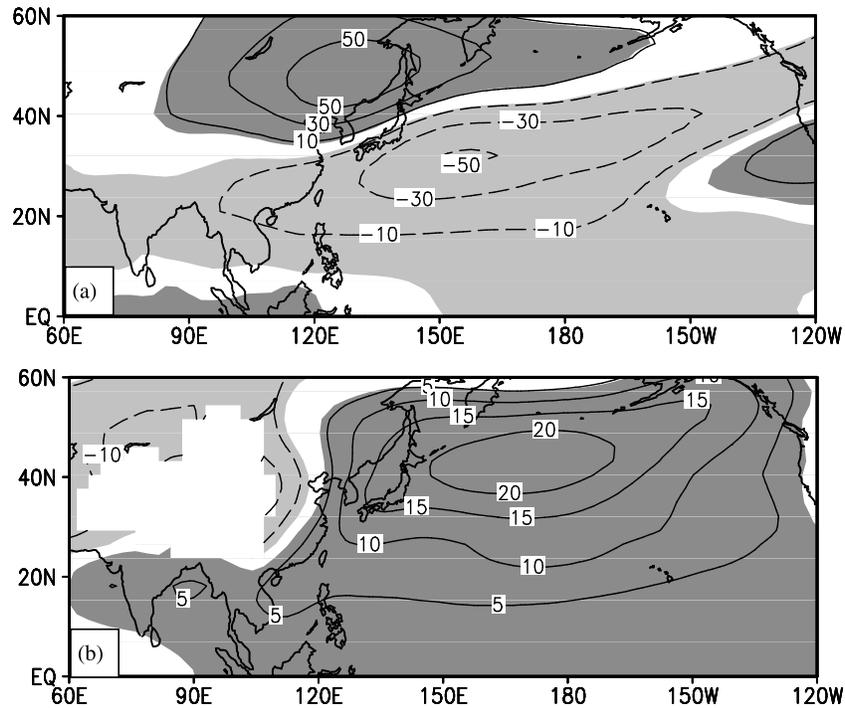
[16] Summing up, compared to the present, the modeling upper tropospheric T' increased over East Asia and decreased over the midlatitudes of the North Pacific in the mid-Holocene, which indicates the strengthened APO. Studies on the modern climate proposed that the forming of APO is associated with an extratropical zonal vertical circulation over the Asian Pacific region. Through this vertical circulation, the Tibetan elevated heating may enhance the tropospheric temperature and upward motion in Asia and then strengthen the downward motion and decrease the tropospheric temperature over the North Pacific [*Zhao et al.*, 2008, 2009]. Therefore, corresponding to the increased Tibetan heating, the APO tends to intensify. Because of the orbital difference between the mid-Holocene and the present, the summer solar radiative heating over the Tibetan Plateau increased in the mid-Holocene relative to the present [*Otto-Bliesner et al.*, 2006; *Wu et al.*, 2006; *Braconnot et al.*, 2007a], which enhanced the upward motion over East Asia and the downward motion over the North Pacific and, consequently, resulted in the intensification of the mid-Holocene APO. Of course, this mechanism is one candidate, and other physical processes may also be responsible for this change of APO.

3.2. Dynamic Linkage of Atmospheric Circulation and Precipitation to the Upper Tropospheric Temperature Change

[17] Corresponding to the change of the upper tropospheric thermal contrast between East Asia and the North

Figure 4. Time series of the simulated Asian Pacific oscillation index (APOI) (top), East Asian T' index (EAI) (middle), and North Pacific T' index (NPI) (bottom). Red (green) lines indicate the temporal change of EAI, NPI, and APOI in the 6ka (0ka) simulations, and blue (yellow) lines indicate their respective mean values.

Figure 5. Composite difference of the summer H' (in m) between 6ka and 0ka at (a) 200 hPa and (b) 850 hPa. Areas above 95% significance level are shaded.

Pacific, there are significant variations of large-scale atmospheric circulation over the Asian Pacific region. Figure 5 manifests the composite difference of the summer eddy geopotential height H' between 6ka and 0ka, in which H' is the deviation of the geopotential height from its zonal mean. Compared to the present, H' increased (decreased) in the upper troposphere and decreased (increased) in the lower troposphere over East Asia (the extratropical North Pacific) during the mid-Holocene because of the local warmer (colder) upper tropospheric T'. This linkage between temperature and geopotential height agrees with the static equilibrium relationship.
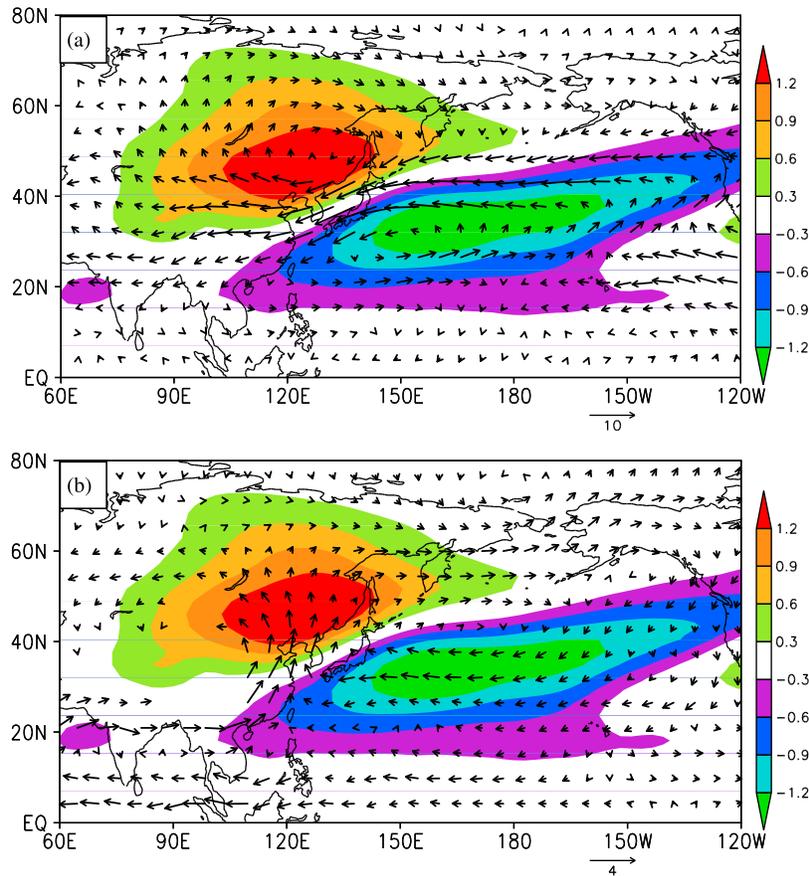
[18] Because we cannot obtain the entire tropospheric temperature data from other models in PMIP2, (such as GISSmodelE, from Goddard Institute for Space Studies; FOAM, Fast Ocean Atmosphere Model; ECHAM5-MPIOM1, Max Planck Institute Ocean Model; MRI-CGCM2.3.4(n)fa, Meteorological Research Institute Coupled General Circulation Model with (without) flux adjustments; MIROC3.2, Model for Interdisciplinary Research Climate 3.2; CSIRO-Mk3L-1.0, -1.1, Commonwealth Scientific and Industrial Research Organization Mk3L Climate System Model versions 1.0 and 1.1), we simply analyze the H' change between 6ka and 0ka for these models. The results show that those features in geopotential height simulated by CCSM3 can also be generally reproduced by these models in PMIP2, although there are quantitative differences in intensity among the models (figures not shown).

[19] Consistent with the changes of geopotential height, a high-level anticyclonic (cyclonic) circulation difference (Figure 6a) and a low-level cyclonic (anticyclonic) circulation difference (Figure 6b) appear over Asia (the North Pacific). The southerly difference prevails in the lower troposphere over East Asia, signifying a stronger East Asian

summer monsoon circulation in the mid-Holocene relative to the present.

[20] The composite difference of the summer 850–500 hPa mean vertical velocity between 6ka and 0ka simulations is displayed in Figure 7, indicating a significant negative difference over East Asia and a significant positive difference over a large area of the North Pacific. This result suggests anomalous upward (downward) motion over East Asia (the North Pacific) in the mid-Holocene as compared to the present. The changes in vertical motion exert impacts on the local precipitation. As indicated by Figure 8, the precipitation generally increased over the East Asian land in the mid-Holocene relative to the present, except for a decrease in the region from the coast of eastern China to Japan. Over the North Pacific, corresponding to the negative and positive H' differences between 6ka and 0ka simulations, respectively, in the upper troposphere and lower troposphere (Figure 5), the high-level Pacific trough and the low-level subtropical high intensified in the mid-Holocene. Such an atmospheric circulation structure often leads to descending over the North Pacific (Figure 7), not favoring the occurrence of precipitation. Thus, the rainfall over the North Pacific is generally reduced in the mid-Holocene compared to the present (Figure 8).

[21] Reconstructions of the mid-Holocene paleoenvironments from pollen-based biome [*Prentice et al.*, 2000] and lake-level data [*Kohfeld and Harrison*, 2000] may be used as key benchmarks for the model evaluation [*Joussaume et al.*, 1999; *Liu et al.*, 2004; *Zheng et al.*, 2004]. Both vegetation [*Yu et al.*, 1998, 2000] and lake data [*Kohfeld and Harrison*, 2000; *Xue and Yu*, 2000; *Wanner et al.*, 2008] show wetter conditions in northern and central China in the mid-Holocene compared to the present. Besides, the lake data suggest that the mid-Holocene was somewhat drier than the
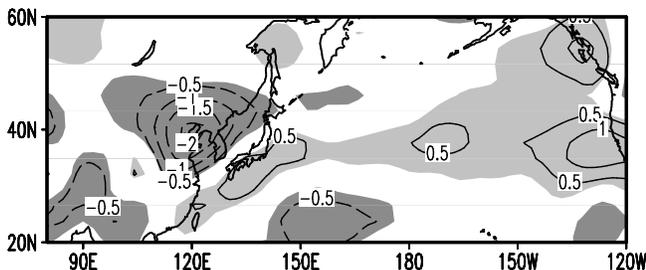
Figure 6. Composite difference of the summer winds (in m/s) between 6ka and 0ka at (a) 200 hPa and (b) 850 hPa. The color shading denotes the upper tropospheric *T'* changes (6ka minus 0ka).
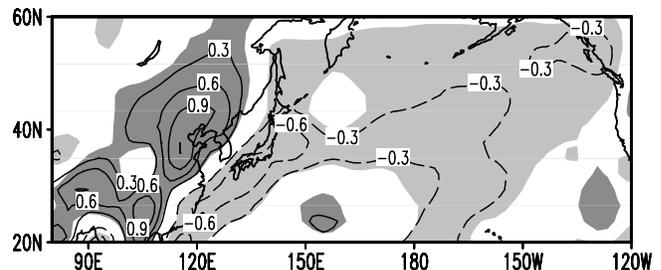
present along the coast of southern China [*Kohfeld and Harrison*, 2000; *Yu et al.*, 2001]. Pollen records reveal that the vegetation patterns were unchanged compared to the present in this region, which is probably because of the fact that the local vegetation is more sensitive to temperature changes than to the moderate decreases in precipitation indicated by the lakes [*Ni et al.*, 2010]. Because there are few dry/wet records over the North Pacific in the mid-Holocene, a comparison between the simulated and observed precipitation results over the North Pacific needs to be done in the future.

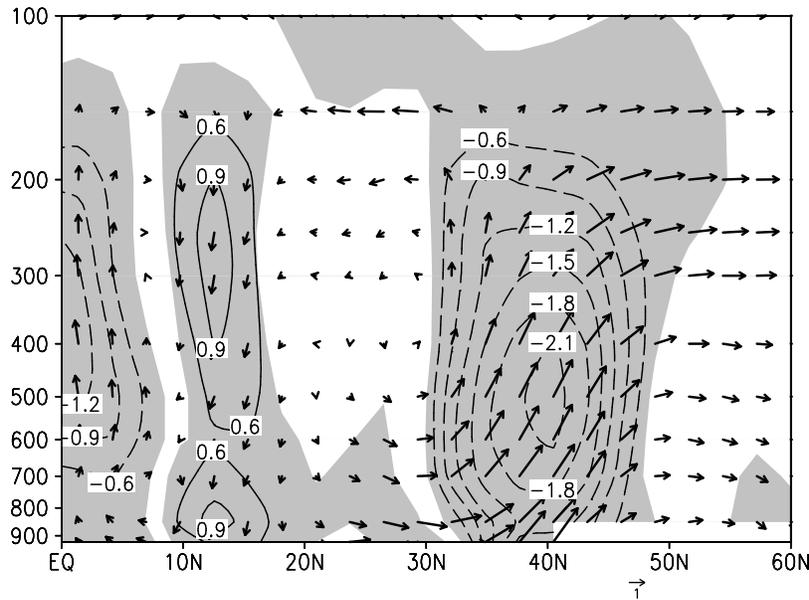[22] Figure 9 shows the latitude-height cross section of the meridional circulation difference along 110–120°E between 6ka and 0ka simulations. It is found that the ascending difference appears between 30 and 50°N, and the descending difference emerges between 10 and 30°N, concomitant with the northerly difference in the upper troposphere and the southerly difference in the lower troposphere. The ascending motion within the latitudes 30–50°N helps to enhance the convective activity. Moreover, the low-level southerly difference favors the water vapor to transport northward. As seen from Figure 10, more water vapor is transported from southern China toward northern China at 6ka than at 0ka, which implies more plentiful summer moisture in the mid-Holocene and favors the increase of precipitation in northern China (shown in Figure 8). Meanwhile, the descending dif-

Figure 7. Composite difference of the summer 850–500 hPa mean vertical velocity (in 10^{-2} Pa/s) between 6ka and 0ka. Areas above 95% significance level are shaded.

Figure 8. Composite difference of the summer precipitation (in mm/d) between 6ka and 0ka. Areas above 95% significance level are shaded.

Figure 9. Latitude-height cross section of the composite difference of the summer meridional wind (in m/s) and vertical velocity (in 10^{-2} Pa/s) between 6ka and 0ka along 110–120°E. The contour denotes the vertical velocity, and the shading indicates the vertical velocity difference above 95% significance level.
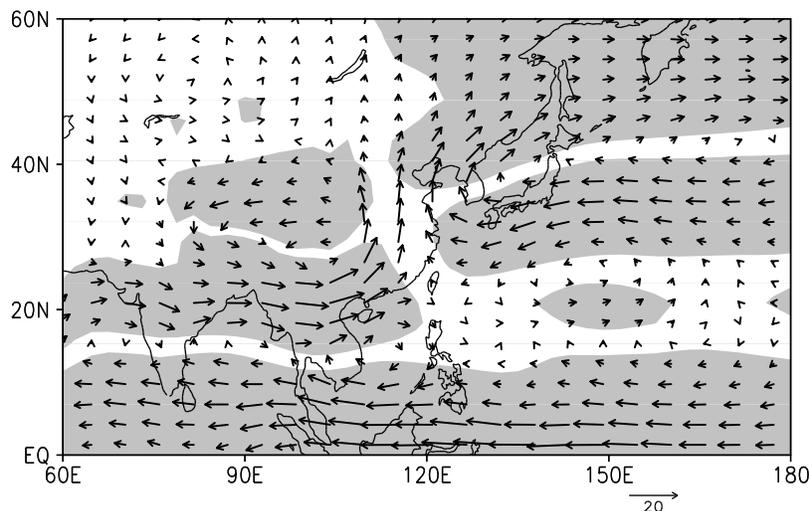
ference appears to the south of 30°N, responsible for the decrease of the local rainfall.

[23] Table 1 shows the correlation coefficients of the upper tropospheric T' or northern China rainfall index with the V_{850} or $\omega_{850-500}$. The northern China rainfall index (NCRI), V_{850} and $\omega_{850-500}$, is respectively defined as the mean precipitation, the 850 hPa meridional wind, and the 850–500 hPa mean vertical velocity over the region (110–120°E, 33–45°N). The NCRI has significant correlations with the V_{850} and $\omega_{850-500}$, with the correlation coefficients of 0.58 (0.61) and −0.86 (−0.83) at 6ka (0ka), respectively. It indicates the low-level southerly wind and the tropospheric upward motion are decisive on the rainfall in northern China. The V_{850} and $\omega_{850-500}$ also have significant

correlations (exceeding the 99% significance level) with the EAI, NPI, and APOI at 6ka (0ka), further demonstrating a close linkage of the low-level meridional wind and the tropospheric vertical motion to the upper tropospheric T'. Therefore, the upper tropospheric T' changes may lead to excessive precipitation in northern China during the mid-Holocene through affecting the low-level meridional wind and the tropospheric vertical motion.

4. Conclusion and Discussion

[24] Using the output from the CCSM3 model, we have investigated the upper tropospheric temperature change between the mid-Holocene and the present. The simulation

Figure 10. Composite difference of the summer 850–500 hPa mean water vapor transport flux (in m s^{-1} g kg^{-1}) between 6ka and 0ka. Areas above 95% significance level are shaded.

Table 1. Correlation Coefficients of V_{850} or $\omega_{850-500}$ With the Upper Tropospheric T' Indices or Northern China Rainfall Index (NCRI)[a]

	V_{850} (110–125°E, 33–45°N)		$\omega_{850-500}$ (110–125°E, 33–45°N)	
	6ka	0ka	6ka	0ka
EAI	0.31	0.36	−0.26	−0.46
NPI	−0.41	−0.54	0.40	0.52
APOI	0.42	0.52	−0.39	−0.58
NCRI	0.58	0.61	−0.86	−0.83

[a]EAI, East Asian T' index; NPI, North Pacific T' index; APOI, Asian Pacific oscillation.

result shows that there existed an out-of-phase relationship in the variability of upper tropospheric T' between East Asia and the extratropical North Pacific in the mid-Holocene. When the upper tropospheric T' increased (decreased) over East Asia, the upper tropospheric T' tended to decrease (increase) over the midlatitudes of the North Pacific. This pattern is consistent with the APO phenomenon obtained from the observation and similar to the modeling result at the present, although there are some differences in intensity.

[25] The definition of the APO index in this study, slightly different from that of the present climate [*Zhao et al.*, 2007], can indicate variability of the thermal contrast between East Asia and the extratropical North Pacific, particularly suitable for modeling the mid-Holocene feature. In comparison with the modern condition, the simulated upper tropospheric T' was warmer over East Asia and colder over the midlatitudes of the North Pacific. Thus, the modeling APO was stronger in the mid-Holocene compared to the present.

[26] The dynamic role of the upper tropospheric T' change in atmospheric circulation and precipitation during the mid-Holocene is preliminarily identified. Corresponding to the stronger APO in the mid-Holocene, the geopotential height increased (decreased) in the upper troposphere and decreased (increased) in the lower troposphere over East Asia (the North Pacific). Accordingly, high-level anticyclonic (cyclonic) circulation and low-level cyclonic (anticyclonic) circulation differences appeared over East Asia (the North Pacific) in the mid-Holocene relative to the present. As a consequence, the ascending motion and the low-level southerly wind strengthened in northern China, conducive to the increase of the local rainfall in the mid-Holocene. Over the North Pacific, the subsiding difference constrained convective activities, leading to deficient precipitation at that time.

[27] Therefore, the summer upper tropospheric T' oscillation in the mid-Holocene is closely associated with the changes of atmospheric circulation and precipitation over the Asian Pacific region, generally consistent with that from the modern climate [*Zhao et al.*, 2007]. This consistency implies that the effects of the summer zonal thermal contrast between Asia and the North Pacific on the East Asian summer monsoonal precipitation occur not only at the present but also in the mid-Holocene.

[28] The APO pattern also occurs in spring [*Zhao et al.*, 2008; *Nan et al.*, 2009]. We have noticed that the spring APO intensity during the mid-Holocene differed from the present. However, its dynamical effects on the spring climate over the Asian Pacific region are not clear. Moreover, the observational studies on the modern climate [*Zhao et al.*,

2009; *Zhou and Zhang*, 2009] have detected a similar out-of-phase relationship in the upper tropospheric temperature between North Africa and the North Atlantic, which may be expected to have effects on the mid-Holocene summer monsoon circulation and climate in North Africa. These issues should be addressed in future work.

References

Berger, A. L. (1978), Long-term variations of caloric insolation resulting from the Earth's orbital elements, *Quat. Res.*, 9, 139–167.

Bonfils, C., N. de Noblet, J. Guiot, and P. Bartlein (2004), Some mechanisms of mid-Holocene climate change in Europe, inferred from comparing PMIP models to data, *Clim. Dyn.*, 23, 79–98.

Braconnot, P., O. Marti, S. Joussaume, and Y. Leclainche (2000), Ocean feedback in response to 6 kyr BP insolation, *J. Clim.*, 13, 1537–1553.

Braconnot, P., et al. (2007a), Results of PMIP2 coupled simulations of the mid-Holocene and last glacial maximum, Part 1: Experiments and large-scale features, *Clim. Past*, 3, 261–277.

Braconnot, P., et al. (2007b), Results of PMIP2 coupled simulations of the mid-Holocene and last glacial maximum, Part 2: Feedbacks with emphasis on the location of the ITCZ and mid- and high latitudes heat budget, *Clim. Past*, 3, 279–296.

Chen, L. X., Q. G. Zhu, H. B. Luo, J. H. He, M. Dong, and Z. Q. Feng (1991), *East Asian Monsoon*, pp. 1–362, Meteorol. Press, Beijing.

Claussen, M., and V. Gayler (1997), The greening of the Sahara during the mid-Holocene: Results of an interactive atmosphere-biome model, *Global Ecol. Biogeogr. Lett.*, 6, 369–377.

Coe, M. T., and S. P. Harrison (2002), The water balance of northern Africa during the mid-Holocene: An evaluation of the 6 ka BP PMIP simulations, *Clim. Dyn.*, 19, 155–166.

Collins, W. D., et al. (2006a), The Community Climate System Model version 3 (CCSM3), *J. Clim.*, 19, 2122–2143.

Collins, W. D., et al. (2006b), The formulation and atmospheric simulation of the Community Atmosphere Model version 3 (CAM3), *J. Clim.*, 19, 2144–2161.

Dallmeyer, A., M. Claussen, and J. Otto (2010), Contribution of oceanic and vegetation feedbacks to Holocene climate change in monsoonal Asia, *Clim. Past*, 6, 195–218.

de Noblet, N., P. Braconnot, S. Joussaume, and V. Masson (1996), Sensitivity of simulated Asian and African summer monsoons to orbitally induced variations in insolation 126, 115 and 6 kBP, *Clim. Dyn.*, 12, 589–603.

Gent, P. R., F. O. Bryan, G. Danabasoglu, K. Lindsay, D. Tsumune, M. W. Hecht, and S. C. Doney (2006), Ocean chlorofluorocarbon and heat uptake during the twentieth century in the CCSM3, *J. Clim.*, 19, 2366–2381.

Hall, N. M. J., and P. J. Valdes (1997), A GCM simulation 6000 years ago, *J. Clim.*, 10, 3–17.

Harrison, S. P., et al. (1998), Intercomparison of simulated global vegetation distributions in response to 6 kyr BP orbital forcing, *J. Clim.*, 11, 2721–2742.

He, J. H., J. H. Ju, Z. P. Wen, J. M. Lü, and Q. H. Jin (2007), A review of recent advances in research on Asian monsoon in China, *Adv. Atmos. Sci.*, 24, 972–992.

Hewitt, C. D., and J. F. B. Mitchell (1998), A fully coupled GCM simulation of the mid-Holocene, *Geophys. Res. Lett.*, 25(3), 361–364, doi:10.1029/97GL03721.

Jolly, D., et al. (1998), Biome reconstruction from pollen and plant macrofossil data for Africa and the Arabian Peninsula at 0 and 6000 years, *J. Biogeogr.*, 25, 1007–1027.

Joussaume, S., et al. (1999), Monsoon changes for 6000 years ago: results of 18 simulations from the Paleoclimate Modeling Intercomparison Project (PMIP), *Geophys. Res. Lett.*, 26(7), 859–862, doi:10.1029/1999GL900126.

Kohfeld, K. E., and S. P. Harrison (2000), How well can we simulate past climates? Evaluating the models using global palaeoenvironmental datasets, *Quat. Sci. Rev.*, *19*, 321–346.

Kutzbach, J. E., and P. J. Guetter (1986), The influence of changing orbital parameters and surface boundary conditions on climate simulations for the past 18,000 years, *J. Atmos. Sci.*, *43*, 1726–1759.

Kutzbach, J. E., and Z. Liu (1997), Response of the African monsoon to orbital forcing and ocean feedbacks in the middle Holocene, *Science*, *278*, 440–443.

Kutzbach, J. E., G. Bonan, J. Foley, and S. P. Harrison (1996), Vegetation and soil feedbacks on the response of the African monsoon to orbital forcing in the early to middle Holocene, *Nature*, *384*, 623–626.

Levis, S., G. B. Bonan, and C. Bonfils (2004), Soil feedback drives the mid-Holocene North African monsoon northward in fully coupled CCSM2 simulations with a dynamic vegetation model, *Clim. Dyn.*, *23*, 791–802.

Liu, Z., E. C. Brady, and J. Lynch-Stieglitz (2003a), Global ocean response to orbital forcing in the Holocene, *Paleoceanography*, *18*(2), 1041, doi:10.1029/2002PA000819.

Liu, Z., B. Otto-Bliesner, J. Kutzbach, L. Li, and C. Shields (2003b), Coupled climate simulation of the evolution of global monsoons in the Holocene, *J. Clim.*, *16*, 2472–2490.

Liu, Z., S. P. Harrison, J. Kutzbach, and B. Otto-Bliesner (2004), Global monsoons in the mid-Holocene and oceanic feedback, *Clim. Dyn.*, *22*, 157–182.

Marzin, C., and P. Braconnot (2009a), Variations of Indian and African monsoons induced by insolation changes at 6 and 9.5 kyr BP, *Clim. Dyn.*, *33*, 215–231.

Marzin, C., and P. Braconnot (2009b), The role of the ocean feedback on Asian and African monsoon variations at 6 kyr and 9.5 kyr BP, *C. R. Geosci.*, *341*, 643–655.

Nan, S., P. Zhao, S. Yang, and J. Chen (2009), Springtime tropospheric temperature over the Tibetan Plateau and evolutions of the tropical Pacific SST, *J. Geophys. Res.*, *114*, D10104, doi:10.1029/2008JD011559.

Ni, J., Y. Ge, S. P. Harrison, and I. C. Prentice (2010), Palaeovegetation in China during the late Quaternary: Biome reconstructions based on a global scheme of plant functional types, *Palaeogeogr. Palaeoclimatol. Palaeoecol.*, *289*, 44–61.

Ohgaito, R., and A. Abe-Ouchi (2007), The role of ocean thermodynamics and dynamics in Asian summer monsoon changes during the mid-Holocene, *Clim. Dyn.*, *29*, 39–50.

Otto-Bliesner, B. L., E. C. Brady, G. Clauzet, R. Tomas, S. Levis, and Z. Kothavala (2006), Last glacial maximum and Holocene climate in CCSM3, *J. Clim.*, *19*, 2526–2544.

Prentice, I. C., D. Jolly, and Biome 6000 Participants (2000), Mid-Holocene and glacial-maximum vegetation geography of the northern continents and Africa, *J. Biogeogr.*, *27*, 507–519.

Rennsen, H., H. Goosse, T. Fichefet, V. Brovkin, E. Driesschaert, and F. Wolk (2005), Simulating the Holocene climate evolution at northern high latitudes using a coupled atmosphere-sea ice-ocean-vegetation model, *Clim. Dyn.*, *24*, 23–43.

Uppala, S. M., et al. (2005), The ERA-40 reanalysis, *Q. J. R. Meteorol. Soc.*, *131*, 2961–3012.

Voss, R., and U. Mikolajewicz (2001), The climate of 6000 years BP in near-equilibrium simulations with a coupled AOGCM, *Geophys. Res. Lett.*, *28*(11), 2213–2216, doi:10.1029/2000GL012498.

Wang, H. J. (1999), Role of vegetation and soil in the Holocene megathermal climate over China, *J. Geophys. Res.*, *104*(D8), 9361–9367, doi:10.1029/1999JD900049.

Wang, H. J. (2000), The seasonal climate and low frequency oscillation in the simulated mid-Holocene megathermal climate, *Adv. Atmos. Sci.*, *17*, 445–457.

Wang, H. J. (2002), The mid-Holocene climate simulated by a grid-point AGCM coupled with a biome model, *Adv. Atmos. Sci.*, *19*, 205–218.

Wang, T., H. J. Wang, and D. B. Jiang (2010), Mid-Holocene East Asian summer climate as simulated by the PMIP2 models, *Palaeogeogr. Palaeoclimatol. Palaeoecol.*, *288*, 93–102.

Wang, Y., M. Notaro1, Z. Liu, R. Gallimore, S. Levis, and J. E. Kutzbach (2008), Detecting vegetation-precipitation feedbacks in mid-Holocene North Africa from two climate models, *Clim. Past*, *4*, 59–67.

Wanner, H., et al. (2008), Mid- to late Holocene climate change: an overview, *Quat. Sci. Rev.*, *27*, 1791–1828.

Wohlfahrt, J., S. P. Harrison, and P. Braconnot (2004), Synergistic feedbacks between ocean and vegetation on mid- and high-latitude climates during the mid-Holocene, *Clim. Dyn.*, *22*, 223–238.

Wohlfahrt, J., S. P. Harrison, P. Braconnot, C. D. Hewitt, A. Kitoh, U. Mikolajewicz, B. L. Otto-Bliesner, and S. L. Weber (2008), Evaluation of coupled ocean-atmosphere simulations of the mid-Holocene using paleovegetation data from the northern hemisphere extratropics, *Clim. Dyn.*, *31*, 871–890.

Wu, Y. H., A. Lücke, Z. D. Jin, S. M. Wang, G. H. Schleser, R. W. Battarbee, and W. L. Xia (2006), Holocene climate development on the central Tibetan Plateau: A sedimentary record from Cuoe Lake, *Palaeogeogr. Palaeoclimatol. Palaeoecol.*, *234*, 328–340.

Xue, B., and G. Yu (2000), Changes of atmospheric circulation since the last interstadial as indicated by the lake-status record in China, *Acta Geol. Sin.*, *74*, 836–845.

Yu, G., and S. P. Harrison (1996), An evaluation of the simulated water balance of Eurasia and northern Africa at 6000 y BP using lake status data, *Clim. Dyn.*, *12*, 723–735.

Yu, G., I. C. Prentice, S. P. Harrison, and X. Sun (1998), Pollen-based biome reconstructions for China at 0 and 6000 years, *J. Biogeogr.*, *25*, 1055–1069.

Yu, G., et al. (2000), Palaeovegetation of China: a pollen data-based synthesis for the mid mid-Holocene and last glacial maximum, *J. Biogeogr.*, *27*, 635–664.

Yu, G., B. Xue, J. Liu, X. Chen, and Y. Q. Zheng (2001), *Lakes evolution in China and paleoclimatic dynamics*, Meteorolog. Press, Beijing, pp. 1–196.

Zhao, P., Y. N. Zhu, and R. H. Zhang (2007), An Asian-Pacific teleconnection in summer tropospheric temperature and associated Asian climate variability, *Clim. Dyn.*, *29*, 293–303.

Zhao, P., J. M. Chen, D. Xiao, S. L. Nan, Y. Zou, and B. T. Zhou (2008), Summer Asian-Pacific oscillation and its relationship with atmospheric circulation and monsoon rainfall, *Acta Meteorol. Sin.*, *22*, 455–471.

Zhao, P., Z. H. Cao, and J. M. Chen (2009), A summer teleconnection over the extratropical Northern Hemisphere and associated mechanisms, *Clim. Dyn.*, doi:10.1007/s00382-009-0699-0.

Zhao, P., S. Yang, and R. C. Yu (2010), Long-term changes in rainfall over Eastern China and large-scale atmospheric circulation associated with recent global warming, *J. Clim.*, *23*, 1544–1562.

Zhao, Y., P. Braconnot, O. Marti, S. P. Harrison, C. Hewitt, A. Kitoh, Z. Liu, U. Mikolajewicz, B. Otto-Bliesner, and S. L. Weber (2005), A multi-model analysis of the role of the ocean on the African and Indian monsoon during the mid-Holocene, *Clim. Dyn.*, *25*, 777–800.

Zheng, Y. Q., G. Yu, S. M. Wang, B. Xue, D. Q. Zhuo, X. M. Zeng, and H. Q. Liu (2004), Simulation of paleoclimate over East Asia at 6 ka BP and 21 ka BP by a regional climate model, *Clim. Dyn.*, *23*, 513–529.

Zhou, B. T., and P. Zhao (2009), Analysis of the coupled simulation result of the seasonal evolution of the southwesterly wind climate over eastern China in the mid-Holocene, *Quat. Sci.*, *29*, 211–220.

Zhou, T. J., and J. Zhang (2009), Harmonious inter-decadal changes of July–August upper tropospheric temperature across the North Atlantic, Eurasian continent and North Pacific, *Adv. Atmos. Sci.*, *26*, 656–665.

P. Zhao, National Meteorological Information Center, China Meteorological Administration, Beijing, China, 100081.

B. Zhou, National Climate Center, China Meteorological Administration, Beijing, China, 100081. (zhoubt@cma.gov.cn)